Aero-thermo-elastic Numerical Calculation and Analysis of Spinning Rocket

Chen Dongyang(陈东阳)[1], *Laith K. Abbas*[1*], *Rui Xiaoting*(芮筱亭)[1], *Marzocca Piergiovanni*[2], *Wang Guoping*(王国平)[1]

1. Institute of Launch Dynamics, Nanjing University of Science and Technology, Nanjing, 210094, P. R. China;
2. Department of Mechanical and Aerospace Engineering, The Wallace H. Coulter School of Engineering, Clarkson University, New York, 13699-5725, USA

(Received 15 May 2013; revised 5 November 2013; accepted 8 November 2013)

Abstract: The application of computational fluid dynamics/computational solid method (CFD/CSM) on solving the aero-thermo-elastic problem of spinning rocket is introduced. Firstly, the aerodynamic coefficients of a rocket are calculated, and the results are compared with the available experimental data, which verified the accuracy of the CFD output. Then, analysis is carried using ANSYS Workbench multi-physics coupling platform, which includes fluid, thermal, and structural solvers. The results show that spinning causes a significant effect on the deformations and stresses. Furthermore, thermal stresses due to high temperature at the rocket warhead and tail edges have a dominated effect, even more than those produced by aerodynamic forces. Consequently, this important outcome should be taken into consideration during the rocket design stages.

Key words: ANSYS Workbench; numerical calculation; thermal stress; spinning

CLC number: V448.15 **Document code**: A **Article ID**: 1005-1120(2014)06-0681-07

1 Introduction

With the development of aerospace technology, all kinds of vehicles speed are constantly increasing. Aerodynamic heating contributes to high temperature and thermal stresses due to high temperature at vehicles′ warhead and tail edges should not be ignored[1,2]. Nowadays, high speed rockets need to be able to bear not only the aerodynamic pressure load, but also the thermal load generated by aerodynamic heating. Since the effects of aerodynamic thermal load are often neglected in rocket aerodynamic design, it is unable to obtain a more accurate analysis of the data and reach an accurate conclusion. For large slenderness ratio wrap around fins spinning rocket, the research on the whole rocket static aero-thermo-elastic problem is more complex than the separate component ones. In summary, the development of an efficient static aero-thermo-elastic analysis in the preliminary design of the whole rocket is necessary. What is more, aero-thermo-elastic analysis relates to interaction of fluid, temperature and stress fields[3,4]. Decoupling calculation method is used in engineering generally[5-7]. One-way coupling method is used in the paper.

2 Initial Conditions

The model used in these calculations is a finned rocket with a slenderness ratio more than 25. The aerodynamic parameters are calculated in different conditions that the angle of attacks are 0°, 4° and 8°, while the Mach numbers are 1, 1.2, 1.5, 2, 2.5, 3, 3.5 and 4, respectively. The far field free stream condition is standard temperature and pressure (101.325 kPa, 288 K). The aero-thermo-elastic problem is calculated in at-

Foundation item: Supported by the National Natural Science Foundation of China (11102089).

* **Corresponding author**: Laith K. Abbas, Professor, E-mail: laithabbas@yahoo.com.

mosphere condition (82.822 5 kPa, 277 K) at a height of 1 300 m. The angles of attack are 0.58°,4°,8°,Mach numbers is 3.4, and the spinning speed is more than 130 rad/s. It is assumed the air is modeled as an ideal gas and the viscosity varies with temperature in accordance with Surthland three coefficient formulas. The internal structure of the rocket is simplified. The shell thickness is assumed as 5 mm and the material is assumed as 30CrMnSi. The internal section of the rocket is divided into multiple segments, and each section maintains the defined density, Poisson's ratio, Young's modulus and coefficient of thermal conductivity. The internal materials are steel, explosive and propellant.

3 Flow Field Calculation Methodology

Computational fluid dynamics (CFD) is used to accurately compute the aerodynamic coefficients of many complex geometry [8-10], and complex flow phenomena[11,12]. The method is used to compute the aerodynamic forces and aerodynamic heating loads. The convective flux use two order upwind and advection upstream splitting method (AUSM) schemes and selecting the shear stress transport (SST) turbulence model[13]. In the paper, the far-field boundary is based on Rieman invariants reflecting boundary conditions. The method of the virtual wall is used to simulate the heat conduction. The single reference frame model is used to perform the problem of spinning supersonic rocket[14]. Flow field mesh number is 1 500 000, $Y^+ \leqslant 2$[15]. Fig. 1 shows the topology graph of fluid filed. Flow field computation grid is shown in Figs. 2, 3.

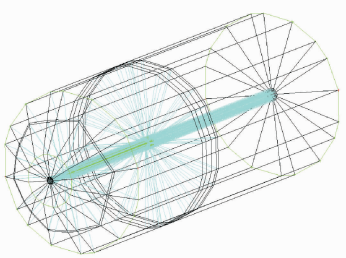

Fig. 1 Topology graph

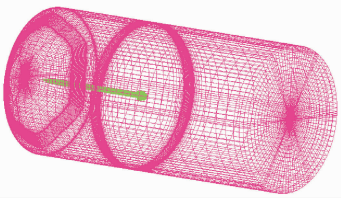

Fig. 2 Flow field grid

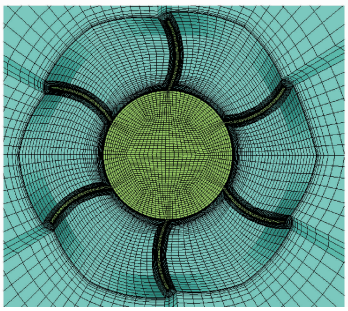

Fig. 3 Section of grid

4 Structure Field Calculation Method

Finite element method is used to calculate the rocket deformations and stress distributions. The rocket solid region grid and simplified internal region grid are shown in Figs. 4, 5. Using the multi point constraint (MPC) approach to define the bonding of contact surfaces, normal force and tangential force of each part are transferred through contact surfaces. ANSYS multi-field solver can be used to deal with the problems that the meshes do not match on the coupling interface. Inertia relief is a method that based on d'Alembert principle, adding a virtual inertial force to balance the external force. It is used to simulate the rocket's free flight condition and make sure that the rocket has no rigid body displacement [16]. In addition, because the body is rotating, a rotating angular velocity is applied to the rocket body.

Fig. 4 Solid region grid

Fig. 5 Internal region grid

5 Equations

5.1 Aerodynamic flow

The general form of the fluid dynamics control equation can be expressed as

$$\frac{\partial \boldsymbol{Q}}{\partial t}+\frac{\partial \boldsymbol{E}}{\partial x}+\frac{\partial \boldsymbol{F}}{\partial y}+\frac{\partial \boldsymbol{G}}{\partial z}=\frac{\partial \boldsymbol{E}_v}{\partial x}+\frac{\partial \boldsymbol{F}_v}{\partial y}+\frac{\partial \boldsymbol{G}_v}{\partial z} \quad (1)$$

where

$$\boldsymbol{Q}=[\rho,\rho u,\rho v,\rho w,\rho E]^{\mathrm{T}}$$
$$\boldsymbol{E}=[\rho u,\rho u^2+p,\rho uv,\rho uw,(\rho E+p)u]^{\mathrm{T}}$$
$$\boldsymbol{F}=[\rho v,\rho vu,\rho v^2+p,\rho vw,(\rho E+p)v]^{\mathrm{T}}$$
$$\boldsymbol{G}=[\rho w,\rho wu,\rho wv,\rho w^2+p,(\rho E+p)w]^{\mathrm{T}}$$
$$\boldsymbol{E}_v=[0,\tau_{xx},\tau_{xy},\tau_{xz},\beta_x]^{\mathrm{T}}$$
$$\boldsymbol{F}_v=[0,\tau_{yx},\tau_{yy},\tau_{yz},\beta_y]^{\mathrm{T}}$$
$$\boldsymbol{G}_v=[0,\tau_{zx},\tau_{zy},\tau_{zz},\beta_z]^{\mathrm{T}}$$

where ρ is the fluid density, p the pressure, and E the total energy of unit mass. (u,v,w) are the three components of the Cartesian coordinate system. N-S equations of rotating coordinates [14]

$$\frac{\partial \rho}{\partial t}+\frac{\partial}{\partial x_j}(\rho w_j)=0 \quad (2)$$

$$\frac{\partial}{\partial t}(\rho u_i)+\frac{\partial}{\partial x_j}(\rho w_j w_i+p\delta_{ij})=\frac{\partial}{\partial x_j}(\tau_{ij})+\rho F_i \quad (3)$$

$$\frac{\partial}{\partial t}(\rho E')+\frac{\partial}{\partial x_j}(\rho w_j E'+w_j p)=\frac{\partial}{\partial x_j}(w_i\tau_{ij}+k\frac{\partial T}{\partial x_j})+\rho\bar{q}+\rho f_i w_i \quad (4)$$

where

$$\tau_{ij}=\mu\left[\left(\frac{\partial w_i}{\partial x_j}+\frac{\partial w_j}{\partial x_i}\right)-\frac{2}{3}\delta_{ij}\frac{\partial w_k}{\partial x_k}\right]$$
$$F_i=f_i-2e_{ijk}\omega_j w_k+\frac{\partial}{\partial x_j}\left(\frac{\omega^2R^2}{2}\right)$$
$$E'=e+\frac{W^2}{2}-\frac{\omega^2R^2}{2}=\frac{P}{\rho(\gamma-1)}+\frac{W^2}{2}-\frac{\omega^2R^2}{2}$$

where W is the relative speed, E' the total energy of relative rotation, $\bar{q}$ the radiant heat ($\bar{q}=0$ in the present study), F the external force, including volume force and centrifugal force, ω the angular velocity of rotation, and R the radius of gyration.

For the closure of above equations, the SST k-ω turbulence model developed by Menter[13] is used. The SST model integrates the advantages of standard k-ε and standard k-ω model boundary layer inside and outside. k and ω transport equation can be written as[13]

$$\frac{\mathrm{d}(\rho k)}{\mathrm{d}t}=\tau_{ij}\frac{\partial u_i}{\partial x_j}-\beta^*\rho\omega k+\frac{\partial}{\partial x_j}\left[(\mu+\sigma_k\mu_t)\frac{\partial k}{\partial x_j}\right] \quad (5)$$

$$\frac{\mathrm{d}(\rho\omega)}{\mathrm{d}t}=\frac{\gamma\rho}{\mu_t}\tau_{ij}\frac{\partial u_i}{\partial x_j}-\beta\rho\omega^2+\frac{\partial}{\partial x_j}\left[(\mu+\sigma_\omega\mu_t)\frac{\partial \omega}{\partial x_j}\right]+2\rho(1-F_1)\sigma_{\omega2}\frac{1}{\omega}\frac{\partial k}{\partial x_j}\frac{\partial \omega}{\partial x_j} \quad (6)$$

where τ_{ij} is shear stress

$$\tau_{ij}=\mu_t\left(\frac{\partial u_i}{\partial x_j}+\frac{\partial u_j}{\partial x_i}-\frac{2}{3}\frac{\partial u_k}{\partial x_k}\delta_{ij}\right)-\frac{2}{3}\rho k\delta_{ij} \quad (7)$$

Blending function F_1

$$F_1=\tanh(\arg_1^4) \quad (8)$$

where

$$\arg_1=\min\left[\max\left(\frac{\sqrt{k}}{0.09\omega y},\frac{500\upsilon}{y^2\omega}\right),\frac{4\rho\sigma_{\omega2}k}{CD_{k\omega}y^2}\right]$$
$$CD_{k\omega}=\max\left(2\rho\sigma_{\omega2}\frac{1}{\omega}\frac{\partial k}{\partial x_j}\frac{\partial \omega}{\partial x_j},10^{-20}\right)$$

The eddy viscosity is defined as

$$\mu_t=\frac{\rho\alpha_1 k}{\max(\alpha_1\omega,\Omega F_2)} \quad (9)$$

where Ω is the absolute value of the vorticity, and F_2 given by

$$F_2=\tanh(\arg_2^2) \quad (10)$$

where $\arg_2=\max\left(\frac{2\sqrt{k}}{0.09\omega y},\frac{500\mu}{\rho y^2\omega}\right)$.

The constants φ of the SST model are calculated from the constants, φ_1,φ_2 as follows

$$\varphi=F_1\varphi_1+(1-F_1)\varphi_2 \quad (11)$$

where φ_1 is the constants of k-ω model, φ_2 the constants of k-ε model.

The constant set φ_1 is

$$\sigma_{k1}=0.5,\sigma_{\omega1}=0.5,\beta_1=0.075,\beta^*=0.09$$
$$\kappa=0.41,\gamma_1=\left(\frac{\beta_1}{\beta^*}\right)-\left(\frac{\sigma_{\omega1}\kappa^2}{\sqrt{\beta^*}}\right)$$

The constant set φ_2 is

$$\sigma_{k2}=1.0,\sigma_{\omega1}=0.856,\beta_2=0.0828,\beta^*=0.09$$
$$\kappa=0.41,\gamma_2=\left(\frac{\beta_2}{\beta^*}\right)-\left(\frac{\sigma_{\omega2}\kappa^2}{\sqrt{\beta^*}}\right)$$

All other parameters are given in Ref. [13].

5.2 Heat transfer in structure

Fluid-solid coupling heat conduction method can be expressed as[17]

$$\frac{\partial}{\partial t}(\rho h)+\nabla\cdot(v\rho h)=\nabla\cdot(k\nabla T)+S_h \quad (12)$$

where ρ is the density, h the sensible enthalpy, k the thermal conductivity, T the temperature, and S_h the volumetric heat source. Therefore, transient term and heat source are zeros.

5.3 Formulas of aerodynamic coefficients

$$C_d=\frac{F_d}{q_\infty S} \quad (13)$$

$$C_l=\frac{F_l}{q_\infty S} \quad (14)$$

$$C_m=\frac{M}{q_\infty Sl} \quad (15)$$

$$x_{cp}=x_{cg}-\frac{C_m}{C_N} \quad (16)$$

where q_∞, S, x_{cp} and x_{cg} are the dynamic pressure, reference area, center of pressure location and center of gravity location coefficients, respectively. l is the length of the rocket, F_d the drag force, F_l the lift force, M the pitching moment, and C_N the coefficient of normal force. The vertex of the rocket warhead is the reference point.

5.4 Static structure analysis

(1) Steady state thermal analysis equation

$$\boldsymbol{K}(T)\boldsymbol{T}=\boldsymbol{Q}(T) \quad (17)$$

where $\boldsymbol{K}$ is the thermal conduction matrix, and $\boldsymbol{Q}$ the rate of heat flux vector. Two kinds of the thermal element which are 10 nodes tetrahedron element (SOLID87) and 20 nodes hexahedron element (SOLID90) are used to do thermal analysis. Firstly, temperature field is obtained through thermal analysis. Then, temperature field is putted into structure elements to do structure analysis.

(2) Static structure analysis equation

$$\boldsymbol{K\delta}=\boldsymbol{F} \quad (18)$$

where $\boldsymbol{K}$ is the stiffness matrix, $\boldsymbol{\delta}$ the displacement vector, and $\boldsymbol{F}$ the force vector. Two kinds of deluxe structure elements, 10 nodes tetrahedron element (SOLID187) and 20 nodes hexahedron element (SOLID186), are used to do structure analysis. Three kinds of load are applied to these structure elements. They are inertial loads, structure loads and thermal loads.

5.5 Coupling equations

Deformation compatibility conditions and force equilibrium conditions should be satisfied on the fluid-structure coupling interface[18].

$$d_f=d_s \quad (19)$$

$$n\cdot\tau_f=n\cdot\tau_s \quad (20)$$

$$q_f=q_s \quad (21)$$

$$T_f=T_s \quad (22)$$

where d, q, T, and τ are displacement, heat flux, temperature and stress field on the fluid-structure coupling interface, respectively. n is the normal direction of interface. Subscripts f and s represent the fluid and the solid, respectively.

6 Calculation Flow Chart

One-way coupling method is used to calculate the fluid-thermal-structure coupling calculation problem. The one-way method flow chart is shown in Fig. 6.

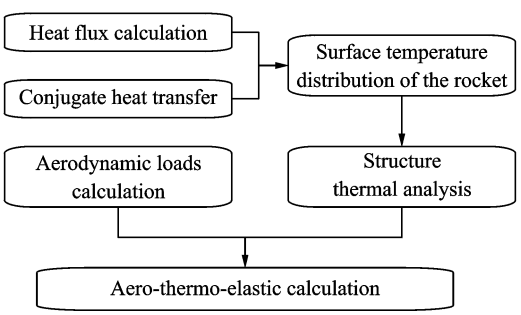

Fig. 6 Aero-thermo-elastic calculation flow chart

7 Numerical Results and Discussion

7.1 Aerodynamic coefficients analysis

The drag, lift, pitching moment and center of pressure coefficients result from implementation of CFD are shown in Figs. 7—10. The results are compared with the experimental data, and illustrate that the SST turbulence model can compute accurately the supersonic rocket aerodynamic forces with high accuracy verifying the accuracy of the CFD numerical results.

7.2 Aerodynamic heating analysis

Fig. 11(a) through Fig. 11(c) are contours of temperature distribution of spinning rocket war-

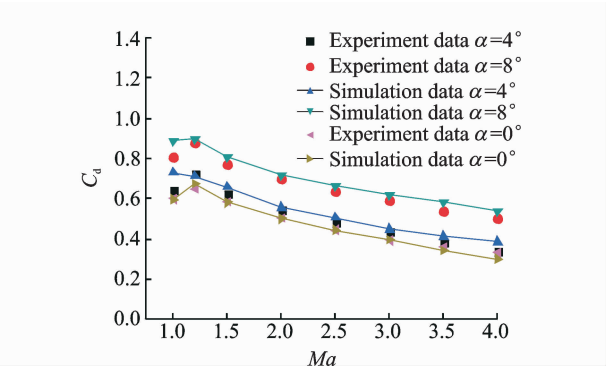

Fig. 7 Drag coefficient v. s. Mach number

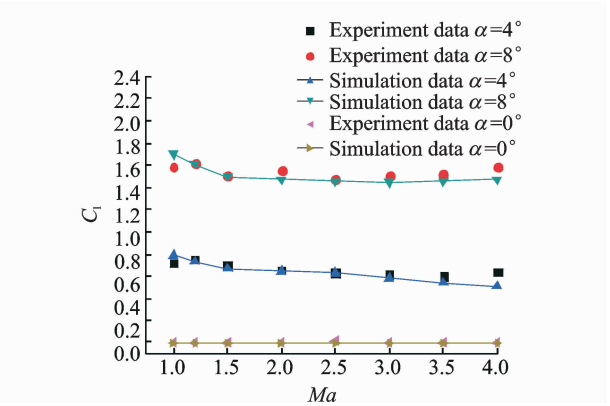

Fig. 8 Lift coefficient v. s. Mach number

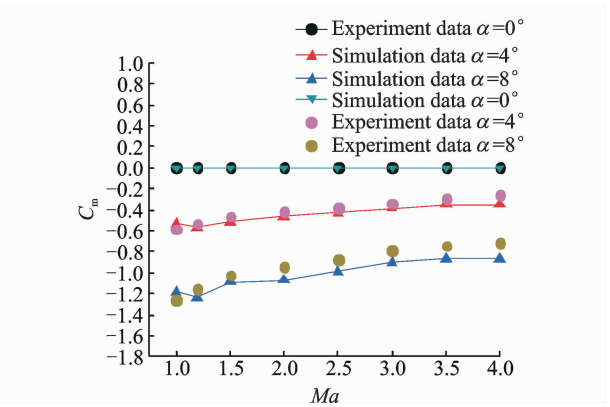

Fig. 9 Pitching moment coefficient v. s. Mach number

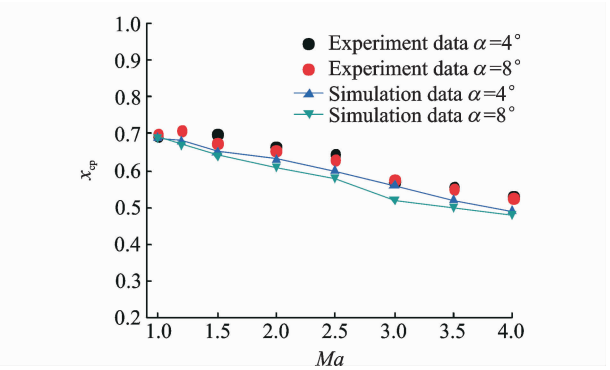

Fig. 10 Center of pressure coefficient v. s. Mach number

head, flow field and fins at $\alpha=0.58°$, respectively. Fig. 11(d) is the contour of a warhead of spinning rocket at $\alpha=8°$. The temperature distribution of center line of windward side and the middle section line of wrap around fin are shown in Figs. 12(a, b), respectively.

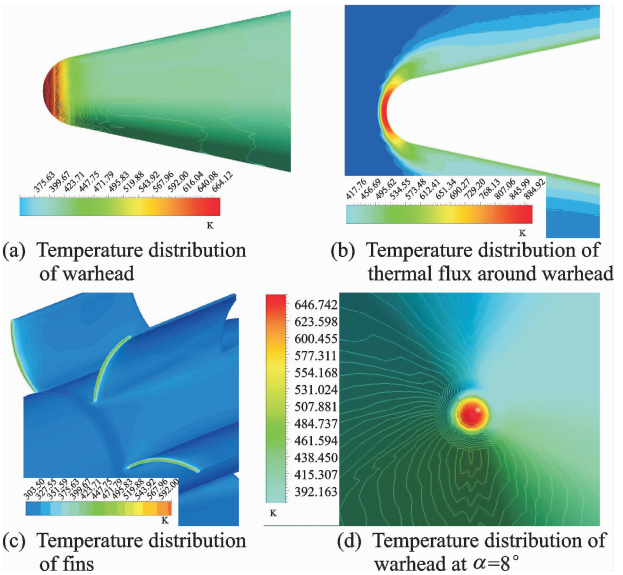

Fig. 11 Contours of rocket temperature

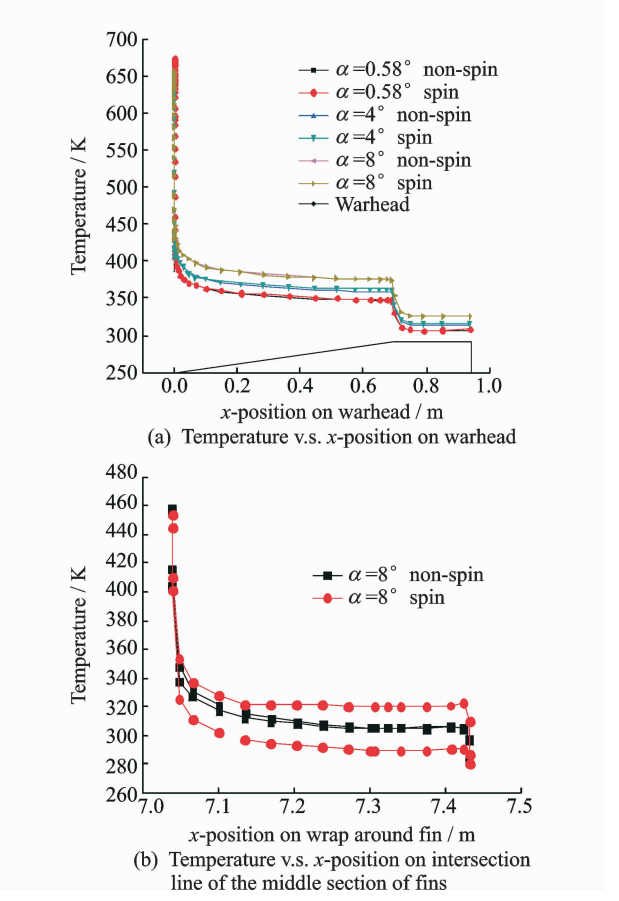

Fig. 12 Curves of temperature distribution

The numerical calculation shows that spinning induces a temperature distribution variation. With increasing the angle of attack, the temperature of windward face becomes higher.

7.3 Aero-thermo-elastic analysis

Figs. 13(a, b) report are the calculation results of the static aeroelasticity for a non-spinning rocket while Figs. 14(a, b) are the results of the thermal-structure coupling of the spinning rocket. The non-spinning aero-elastic one's maximum equivalent stress and total deformation are much smaller than the spinning thermal-structure coupling one. The results demonstrate that aerodynamic heating and spinning have a significant effect on the rocket's deformation.

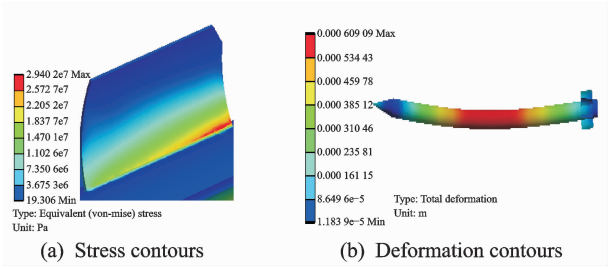

Fig. 13 Stress and deformation contours due to aero-elasticity for non-spinning rocket at $\alpha=0.58°$

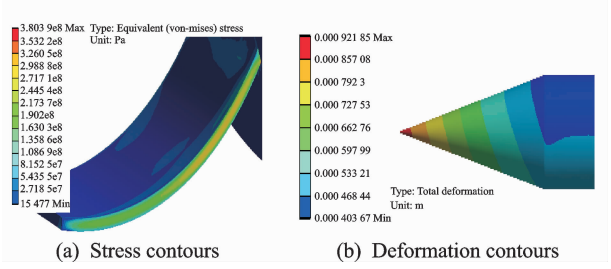

Fig. 14 Stress and deformation contours of thermal-structure coupling of spinning rocket at $\alpha=0.58°$

Table 1 highlights the calculation results of the maximum equivalent stress and total deformation due to the aero-thermal-elastic characteristics of the spinning rocket. It shows that with increasing the angle of attack, the maximum total deformation and equivalent stresses are higher. Since the 30CrMnSi material yields stress of $\sigma_s \geqslant 885$ MPa, the structure of the rocket at these specific flight conditions remains undamaged. However, due to fluid-thermal-structure coupling calculations of the spinning rocket, as shown in Figs. 15, 16, the spinning rocket maximum total deformation due to the first bending mode, occurs in the middle of rocket body, while the maximum equivalent stresses occurs at the bottom of fins. Therefore, a considerable attention should be paid, e.g. fin thermal protection during the manufacturing process.

Table 1 The maximum stress and deformation of spinning rocket

α/(°)	Max equivalent stress/ MPa	Max total deformation/ mm
0.58	415	1.05
4	470	4.82
8	725	6.01

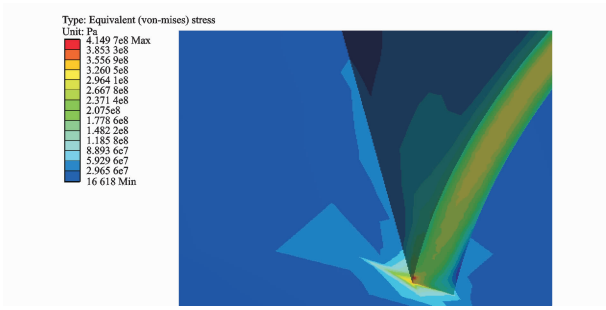

Fig. 15 Stress contour of aero-thermal-elasticity of spinning rocket at $\alpha=0.58°$

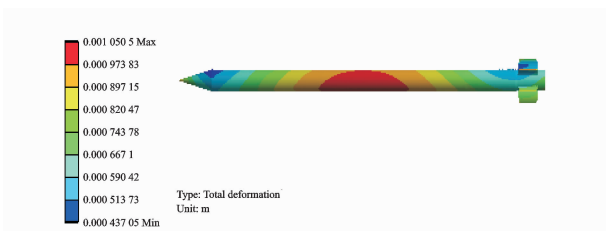

Fig. 16 Total deformation contour of aero-thermal-elasticity of spinning rocket at $\alpha=0.58°$

8 Conclusions

Numerical computations are presented using CFD and CSM to perform aero-thermo-elastic analysis of spinning rocket. For the slender rocket considered, the maximum total deformation is quite small, in the small angle of attack range considered, and the relatively low speed conditions. The fluid-thermal-structure one-way coupling method is demonstrated to the feasible, and the calculation results have shown that spinning

and aerodynamic heating cause a greater effect on the rocket deformations and stresses. In addition, thermal stress can play a significant role. When angles of attack are increasing, the maximum total deformation and equivalent stress are expected to significantly rise. The maximum equivalent stresses occur in the lower part of the fins, while the warhead is exposes to maximum temperature. As a result, it is critical to properly consider thermal protection of the warhead and fins during the rocket manufacturing process.

References:

[1] Li Songnian. Thermomechanical of aerospace structures[J]. Advances in Mechanics, 1994, 24(1):1-22. (in Chinese)

[2] Zhao Xunchuan, Li Songnian, Zhao Tianhui. Thermomechanical analysis in composite wings of guided missile[J]. Journal of Beijing University of Aeronautics and Astronautics, 1996, 22(3): 374-378. (in Chinese)

[3] Bertin J, Cummings R. Fifty years of hypersonics: Where we′ve been, where we′re going [J]. Progress in Aerospace Sciences, 2003, 39(6/7):511-536.

[4] Culler A J, McNamara J J. Studies on fluid-thermal-structural coupling for aerothermoelasticity in hypersonic flow[J]. AIAA Journal, 2010, 48(8):1721-1738.

[5] Kleb Willian. Computational aeroheating predictions for X-34 [J]. Journal of Spacecraft and Rockets, 1999, 36(2):179-188.

[6] Li Xuefei. Numerical simulation of hypersonic aircraft gas thermoelastic multi-field coupling[D]. Harbin: Harbin Institute of Technology, 2011. (in Chinese)

[7] Amundsen Ruth M. Aeroheating thermal model correlation for mars global surveyor solar array [J]. Journal of Spacecraft and Rockets, 2005,42(3): 457-466.

[8] Sahu J, Edge H L, Heavey K R, et al. Computational fluid dynamics modeling of multi-body missile aerodynamic interference, ARL-TR-1765 [R]. [S. l.]: Army Research Lab Aberdeen Proving Ground Md, 1998.

[9] Zhao Pingan. High speed aerodynamic convection and coupled heat transfer of complicated bodies[D]. Harbin: Harbin Institute of Technology, 2008. (in Chinese)

[10] Wu Jun, Guo Zhengqi, Zhong Zhihua. The application of SST turbulence model in the aerodynamic simulation of the automobile[J]. Automotive Engineering, 2003, 25(4): 326-329. (in Chinese)

[11] DeSpirito J, Heavey K R. CFD computation of magnus moment and roll damping moment of a spinning projectile[R]. AIAA-2004-2713, 2004.

[12] DeSpirito J, Plostins P. CFD prediction of M910 projectile aerodynamics: Unsteady wake effect on magnus moment[R]. AIAA-2007-6580, 2007.

[13] Menter F R. Zonal two equation k-ω turbulence models for aerodynamic flows [R]. AIAA-93-2906, 1993.

[14] Deng Fan. Investigations of grid fins aerodynamic shape design and roll characteristics of wing-body configuration[D]. Nanjing: Nanjing University of Science and Technology, 2011. (in Chinese)

[15] Zhang Chenchun, Ren Luquan, Wang Jing. Simulation on flow control for drag reduction of revolution body using bionic dimpled surface [J]. Acta Armament Arii, 2009, 30(8):1066-1071. (in Chinese)

[16] Chen Zhaotao, Sun Qin. Applications of inertia relief method in aircraft static aero-elasticity[J]. Flight Dynamics, 2008, 26(5): 71-74. (in Chinese)

[17] Fluent Inc. Fluent 6.2 user′s guide[M]. Lebanon, NH: Fluent Inc, 2005.

[18] Song Xueguan, Cai Lin, Zhang Hua. ANSYS fluid-structure coupling analysis and engineering examples [M]. Beijing: China Water Power Press, 2012. (in Chinese)

(Executive editor: Xu Chengting)